

UNIVERSITY of CALIFORNIA  
SANTA CRUZ

**THERMAL EVOLUTION OF URANUS AND NEPTUNE WITH  
CONDENSATION-INHIBITED CONVECTION**

A thesis submitted in partial satisfaction of the  
requirements for the degree of

BACHELOR OF SCIENCE

in

ASTROPHYSICS

by

**Robert Schroder**

December 2020

Copyright © by

Robert Schroder

2020

## **Abstract**

Thermal Evolution of Uranus and Neptune with Condensation-inhibited Convection

by

Robert Schroder

We examine under what conditions stable water condensation zones would form in the hydrogen dominated atmospheres of our solar system ice giants. We study these stable condensation zones in the context of an interior structure model that departs from conventional dry-adiabatic models by including a moist adiabatic interior. We investigate how stable water condensation zones impact the warming of the interior, and what impact the presence of these zones have on the thermal evolution of the ice giants. We find that the existence of stable water condensation zones do not explain the problem of Uranus having no intrinsic temperature at present time. We also find that a moist adiabatic interior with the inclusion of stable water condensation zones result in a warmer Uranus and Neptune at present time than predicted by models with simple dry adiabatic or moist adiabatic interiors.

# Contents

<b>List of Figures</b>	<b>v</b>
<b>1 Introduction</b>	<b>1</b>
1.1 Condensation in Hydrogen Dominated Atmospheres . . . . .	4
<b>2 Model</b>	<b>6</b>
2.1 Three-layer Model with Dry Adiabat . . . . .	6
2.2 Inclusion of Moist Adiabat Within Outer Envelope . . . . .	9
2.3 Temperature Jump Across the Water Condensation Zone . . . . .	13
2.4 Energy Conservation and Thermal Evolution of Model . . . . .	14
<b>3 Results</b>	<b>16</b>
3.1 Condensation-inhibited Convection . . . . .	16
3.2 Formation of Radiative Zone . . . . .	17
3.3 Thermal Evolution of Uranus and Neptune . . . . .	19
<b>4 Discussion and Conclusions</b>	<b>27</b>

# List of Figures

2.1	A Standard Interior Structure Model . . . . .	8
2.2	Interior Structure for Moist Adiabat . . . . .	11
2.3	A Standard Interior Structure Model . . . . .	12
3.1	Inhibition of convection on Uranus . . . . .	18
3.2	Impact of Radiative Layer on T10 . . . . .	20
3.3	Formation of Radiative Zone . . . . .	22
3.4	Thermal Evolution Curves for Uranus - Adiabat Comparisons . . . . .	23
3.5	Thermal Evolution Curves for Uranus - Water Vapor Concentration Comparisons . . . . .	24
3.6	Thermal Evolution Curves for Neptune - Water Vapor Concentration Comparisons . . . . .	25
3.7	Thermal Evolution Curves for Uranus - Radius . . . . .	26
3.8	Thermal Evolution Curves for Neptune - Radius . . . . .	26

**1**

# Introduction

Planets coalesce from matter contained in their parent star's protoplanetary disk.

As a planet accretes material from the disk, it heats up, giving the planet a so-called 'hot start'. After accretion is complete, the planet will begin to cool over time. Before proceeding further, it will be helpful to define what we mean by temperature. There are several temperatures that describe a planet's atmosphere. The effective temperature,  $T_{\text{eff}}$ , is defined as the total flux integrated over all frequencies,  $\nu$ , of a black body of the same shape and same distance as the planet (Seager, 2010):

$$\pi \int_0^{\infty} B(T, \nu) d\nu = \sigma_B T_{\text{eff}}^4 \quad (1.1)$$

Here,  $\sigma_B$  is the Stefan-Boltzmann constant, and  $F$  is the solar flux. Simplifying further, this yields

$$T_{\text{eff}} = \left( \frac{F}{\sigma_B} \right)^{\frac{1}{4}}. \quad (1.2)$$

The equilibrium temperature,  $T_{\text{eq}}$ , is the temperature the planet would have if it were in thermal equilibrium with its parent star. This occurs when the planet has radiated away

its latent heat of formation, and the only remaining source of energy is from its star. This temperature is defined as

$$T_{\text{eq}}^4 = \frac{F(1 - A_B)}{r^2 4\pi\sigma_B} \quad (1.3)$$

where  $r$  is the distance from the star in AU,  $A_B$  is the bond albedo. Finally, the intrinsic temperature,  $T_{\text{int}}$ , the temperature that defines the flux from the planet's interior and is defined by the relation

$$T_{\text{eff}}^4 = T_{\text{eq}}^4 + T_{\text{int}}^4. \quad (1.4)$$

In 1965, Frank Low measured Jupiter's intrinsic temperature (Low, 1966). To explain this observation, theorists set out to expand on prior work by (Demarcus, 1958) on the theory of interior structure of solar system gas and ice giants (Hubbard, 1968; Smoluchowski, 1967; Hubbard, 1977, 1978; M. Podolak, 1991). These models assumed that the interior of giant planets are convective, meaning that heat within the planet's interior is transferred by the movement of fluids. In other words, warmer, less dense material will rise; while cooler, more dense material will sink due to the influence of gravity. In 1968, Hubbard showed that a convective interior would allow Jupiter's observed flux to be transported to the surface adiabatically. This analysis motivated the inclusion of adiabatic interiors in contemporary interior structure models for gas and ice giants.

At the present time, most of the giant planets in our solar system: Saturn, Jupiter, and Neptune, all have an intrinsic flux. Uranus is the exception (Pearl & Conrath, 1991). Measurements of Uranus's effective temperature are consistent with a planet that has no intrinsic flux, a planet in thermal equilibrium with the Sun, cooler than its more distant neighbor, Neptune, a planet of similar mass and composition.

While thermal evolution models do currently reproduce  $T_{\text{eff}}$  for Jupiter and Neptune at 4.6 Gyr (Graboske et al., 1975; Fortney et al., 2011), they do not reproduce  $T_{\text{eff}}$  for Saturn and Uranus. Models for Saturn predict a cooler planet; however, plausible explanations have been offered to explain its current, warmer  $T_{\text{eff}}$ . Among them, the rain-out of helium (Fortney & Hubbard, 2003; Mankovich & Fortney, 2019), or double-diffusive convection (Leconte & Chabrier, 2013).

Meanwhile, for Uranus, the models have predicted a warmer effective temperature at present time (Fortney et al., 2011; M. Podolak, 1991; W.B. Hubbard, 1995; L. Scheibe, 2019). There have been various attempts to explain Uranus' cool temperature. Early investigations posited that a stratified interior, stable against convection, would allow heat to be trapped deep within the the interior (M. Podolak, 1991). If in fact, the interior of a planet were stable against against convection, some other means of energy transport must be responsible for transporting heat from the interior to the surface. Possible mechanisms include conduction, radiative diffusion, or perhaps double-diffusive convection. Later work investigated some of the other possible mechanisms for energy transport. (Guillot, 1995) posited that condensates such as  $\text{NH}_3$ ,  $\text{CH}_4$ , or  $\text{H}_2\text{O}$  when at critical abundance could interfere with convection, producing temperature profiles that would be superadiabatic. (Nettelmann et al., 2016) looked at the inclusion of ad-hoc thermal boundary layers within a planet's interior and found that they could possibly explain Uranus's current  $T_{\text{eff}}$ . Both (Friedson & Gonzales, 2017) and (Leconte et al., 2017) explored the impact of condensates forming stable radiative layers. Both carried out linear stability analyses and reached similar findings, concluding that super-critical abundances of  $\text{H}_2\text{O}$  would result in a superadiabatic temperature gradient. Friedson and Gonzales also explored the vulnerability of

these condensation zones to entrainment pressure from the surrounding environment. All of these investigations showed that thermal boundary layers provided a mechanism to trap heat deep within the interior, allowing the envelope above to cool more quickly.

## 1.1 Condensation in Hydrogen Dominated Atmospheres

Up to now, we have discussed convection as a means of energy transport. We have been using terms 'convection' and 'dry convection' synonymously. From here on, we will be explicit. When we speak of dry convection, we are not taking into consideration the condensation of molecular species in the atmosphere. On Earth, the atmosphere undergoes moist convection. As a parcel of air is lifted, it cools until it gets cold enough that water vapor condenses out, releasing latent heat of condensation which further boosts convection. This release of latent heat alters the temperature-pressure profile of the atmosphere, which now follows a moist adiabat. In addition to altering the temperature gradient, condensation may also create a gradient in mean molecular weight. For example, on Earth, moist air is lighter than dry air.  $\text{H}_2\text{O}$  vapor (molecular mass = 18 g/mol), the primary condensate in Earth's atmosphere, is lighter (not by much) than the background air which is composed primarily of  $\text{N}_2$  (molecular mass = 28 g/mol). When  $\text{H}_2\text{O}$  vapor abundance exceeds the saturation vapor pressure, the vapor condenses out of the atmosphere, resulting in a small vertical gradient in mean molecular weight. In Earth's atmosphere, this small gradient does not impose a significant barrier to convection. By contrast, in hydrogen dominated atmospheres such as Neptune and Uranus, the background gas is much lighter than the condensates. In this hydrogen-rich environment, when  $\text{H}_2\text{O}$  condenses out of the atmosphere, a strong vertical gradient in mean molecular weight can be established, resulting

in a negative buoyancy for the convecting parcel of gas. This can create a situation where the zone in which water condenses is stable against convection (Guillot, 1995), (Friedson & Gonzales, 2017), (Leconte et al., 2017). Thus far, we have been discussing H<sub>2</sub>O as the only condensate. However, other condensates such as NH<sub>3</sub> and CH<sub>4</sub> may impact convection as well. In this study, we only consider H<sub>2</sub>O as the primary condensate as it likely has the largest impact. The reason for this is that if its abundance is supercritical, then it results in a larger superadiabicity (larger temperature gradient) than would be provided by either NH<sub>3</sub> r CH<sub>4</sub> (Guillot, 1995). Consideration of other condensates is planned for future work.

The work done by (Guillot, 1995), (Friedson & Gonzales, 2017), and (Leconte et al., 2017) examined under what conditions stable condensation zones would form in hydrogen dominated atmospheres. In this paper, we apply the same physical mechanisms for the formation of stable water condensation zones. However, we expand on this by placing the formation of these stable, radiative layers in the context of a more complete model of interior structure for solar system ice giants. Furthermore, we investigate how these stable layers impact the cooling of the planets over time. In chapter 2, we give a brief description of conventional, dry-convective interior structure models and how our moist-convective model differs. We present our results in Chapter 3, describing where and when stable water condensation zones form, how they impact cooling within the interior, their impact on thermal evolution, and their impact on heat flow at present time. In Chapter 4, we discuss our conclusions and offer suggestions for further work.

# 2

# Model

## 2.1 Three-layer Model with Dry Adiabat

We begin our description of the physics of our interior structure model by assuming spherical symmetry and conservation of mass:

$$\frac{dm}{dr} = 4\pi r^2 \rho \quad (2.1)$$

where  $dm$  is the mass contained within a sphere of radius  $r + dr$ , and  $\rho$  is the density.

Hydrostatic equilibrium is also assumed and described by:

$$\frac{dP}{dr} = -\frac{Gm\rho}{r^2} \quad (2.2)$$

where  $P$  is the pressure and  $G$  is the gravitational constant.

We employ a three-layer interior structure, seen schematically in Figure 2.1. At the center of the planet is a core of mass,  $m_{\text{core}}$ . The core is made of pure water ice, indicated by  $Z = 1$ , the H<sub>2</sub>O mass fraction. Moving outward, the inner envelope is H<sub>2</sub>O

dominated, where  $Z_2$  is the  $\text{H}_2\text{O}$  mass fraction,  $X_2$ , and  $Y_2$  are the hydrogen and helium mass fractions, respectively. The outer envelope, below 1 bar, contains trace amounts of  $\text{H}_2\text{O}$ , but is mostly comprised of hydrogen and helium, with mass fractions equal to  $X_1$  and  $Y_1$ , respectively.  $m_{12}$  is the mass coordinate that indicates the transition between the inner and outer envelope.  $T_1$  is the temperature at  $P = 1$  bar. Near the surface, the ideal gas law provides a good approximation for relating pressure, temperature, density, and composition. However, at depth, this approximation is no longer valid. We use (Chabrier et al., 2019) as our H-He equation of state. For water, we use (S. Mazevert & Potekhin, 2019) EOS.

$X$ ,  $Y$ , and  $Z$  represent mass fractions for hydrogen, helium, and water, respectively.

In general

$$X + Y + Z = 1 \quad (2.3)$$

$Y'$  is the He mass fraction relative to He + H, such that:

$$Y' = \frac{Y}{X + Y} \quad (2.4)$$

We use the additive-volume approximation to determine total density, given by the relation

$$\frac{1}{\rho} = \frac{1 - Z}{\rho_{\text{HHe}}} + \frac{Z}{\rho_Z} \quad (2.5)$$

Internal energy,  $u$ , is given by

$$u = (1 - Z) \times u_{\text{HHe}} + Z \times u_Z \quad (2.6)$$

where

$$u_{\text{HHe}} = (1 - Y') \times u_{\text{H}} + Y' \times u_{\text{He}} \quad (2.7)$$

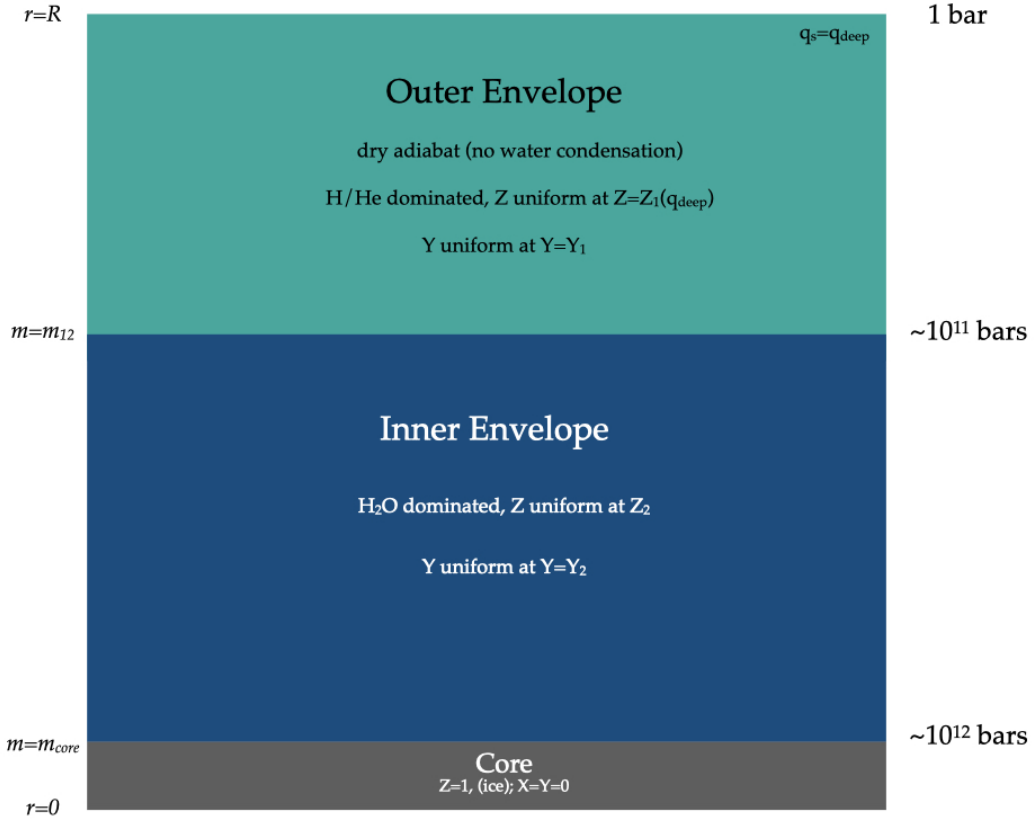


**Figure 2.1:** A conventional interior structure: Fully convective and dry adiabatic. In this model, the inner and outer envelopes are assumed to be well mixed, fully convective, and following a dry adiabat. The core is composed of water ice. The inner envelope is water dominated, with uniform concentrations of hydrogen, helium, and water; whereas, the outer envelope is hydrogen and helium dominated with trace amounts of water. The atmosphere extends beyond 1 bar, but pressures down to 1 bar are sufficient to capture the formation and impact of the water condensation zones investigated here.

Historically, interior structure models have assumed that the interiors are composed of compressible gases that are fully convective. In a dry-convective model such as this, as a parcel of gas rises, its temperature decreases while its volume increases. This process is known as adiabatic expansion. Conversely, if the parcel sinks, it gets warmer as its

volume decreases. This process is known as adiabatic compression. These processes assume constant entropy. While there may be a critical concentration for a condensable species, this dry model does not allow for condensation. It is said that the temperature-pressure profile follows a dry adiabatic gradient (R. Kippenhahn, 2012), given by:

$$\nabla_{\text{ad}} = \left( \frac{\partial \ln T}{\partial \ln P} \right)_s \quad (2.8)$$

where  $s$  is entropy.

Finally, beyond the outer envelope is the atmosphere. Atmospheres regulate how quickly the energy within a planet's interior can radiate into space. When modeling the thermal evolution of gas and ice giants, it has long been recognized that model atmospheres constitute an outer boundary condition for interior structure models, providing key inputs that impact cooling times for interior structure models (Graboske et al., 1975; Fortney et al., 2011). Specifically, model atmospheres allow us to link the planet's  $T_{\text{int}}$  and  $T_{\text{eff}}$  to the model's surface gravity,  $g$ , and its  $T_1$  or  $T_{10}$ . Our work utilizes the (Fortney et al., 2011) model atmosphere.

## 2.2 Inclusion of Moist Adiabat Within Outer Envelope

Our interior structure model modifies the conventional structure described in Section 2.1 by adding a moist adiabatic layer to the outer envelope, which under favorable conditions, allows for the condensation of H<sub>2</sub>O. Gases condense at sufficiently low temperatures or high pressures. Condensation of a gas is characterized by its saturation vapor pressure, which derives from the Clausius-Clapeyron equation (Lavega, 2011). The satura-

tion vapor pressure,  $P_{\text{sat}}$ , is given by

$$P_{\text{sat}}(T) = P_{\text{sat}}(T_0) e^{-\frac{L+C_p T_0}{R_{\text{vap}}}(\frac{1}{T}-\frac{1}{T_0}) - \frac{C_p}{R_{\text{vap}}} \ln \frac{T}{T_0}} \quad (2.9)$$

where  $T_0 = 273.16K$ , and  $R_{\text{vap}}$  is the gas constant for the condensable species. When the partial pressure of a gas,  $P_{\text{gas}}$ , is less than  $P_{\text{sat}}$ , the parcel of gas is 'subsaturated'. When  $P_{\text{gas}} = P_{\text{sat}}$ , the gas is 'saturated'. And, when  $P_{\text{gas}} > P_{\text{sat}}$ , the parcel is 'supersaturated'. Every condensable species has its own saturation vapor pressure. We define the moist adiabat as (Lavega, 2011)

$$\nabla_{\text{moist}} = \left( 1 + \frac{\frac{x_{\text{vap}} L}{R_{\text{vap}} T}}{\nabla_{ad} + \frac{L^2}{R_{\text{vap}}^2 T^2}} \right) \quad (2.10)$$

where

$$x_{\text{vap}} = \frac{P_{\text{sat}}}{P} \quad (2.11)$$

and

$$\frac{dT}{dP} = \frac{T}{P} \nabla_{\text{moist}} \quad (2.12)$$

and the gradient of the water vapor mole fraction is given by

$$\frac{dx_{\text{vap}}}{dP} = \frac{x_{\text{vap}} L}{R_{\text{vap}} T^2} \frac{dT}{dP} - \frac{x_{\text{vap}}}{P} \quad (2.13)$$

In Figure 2.3, we compare pressure-temperature and pressure-xvap profiles that follow a dry adiabatic lapse rate, a moist adiabatic lapse rate, and a moist adiabatic lapse rate containing a radiative layer at some depth. The profile of the moist adiabatic lapse rate is cooler at depth than either of the other two profiles. However, the presence of a stable radiative layer results in a warmer interior. These profiles assume  $q_{\text{deep}} = 0.25$  and  $T_1 = 150K$ , which is approximately when the onset of condensation-inhibited convection occurs, as will be shown in Chapter 3. When the pressure-temperature profile follows a dry adiabat, the vapor mole fraction,  $x_{\text{vap}}$ , is constant.

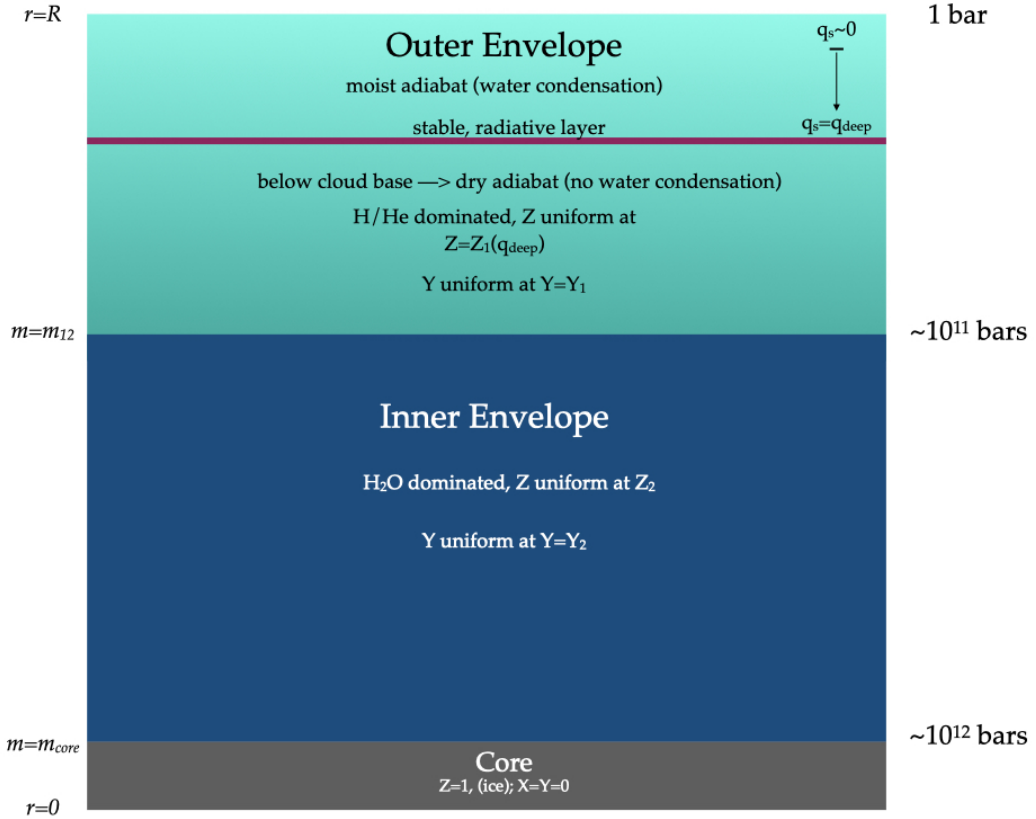


**Figure 2.2:** The structure for moist adiabatic interior, allowing for condensation-inhibited convection. In this model, a stable water condensation zone may form. The red horizontal line indicates the radiative zone (water condensation zone). The pressure and temperature at the base of the condensation zone is set by the condition that  $x_{\text{vap}}$  has reached the deep value  $x_{\text{vap}}^{\text{deep}}$ . Below the condensation zone, the temperature and pressure follow a dry adiabat.

If condensation occurs, our model assumes that it may be stable against convection if a fast rain-out occurs such that the vertical gradient in mean molecular weight is large enough to counteract the positive buoyancy of the parcel of gas (Leconte et al., 2017) (Friedson & Gonzales, 2017). In this scenario, convection is interrupted when  $\alpha$  is negative, where  $\alpha$  (Friedson & Gonzales, 2017) is given by:

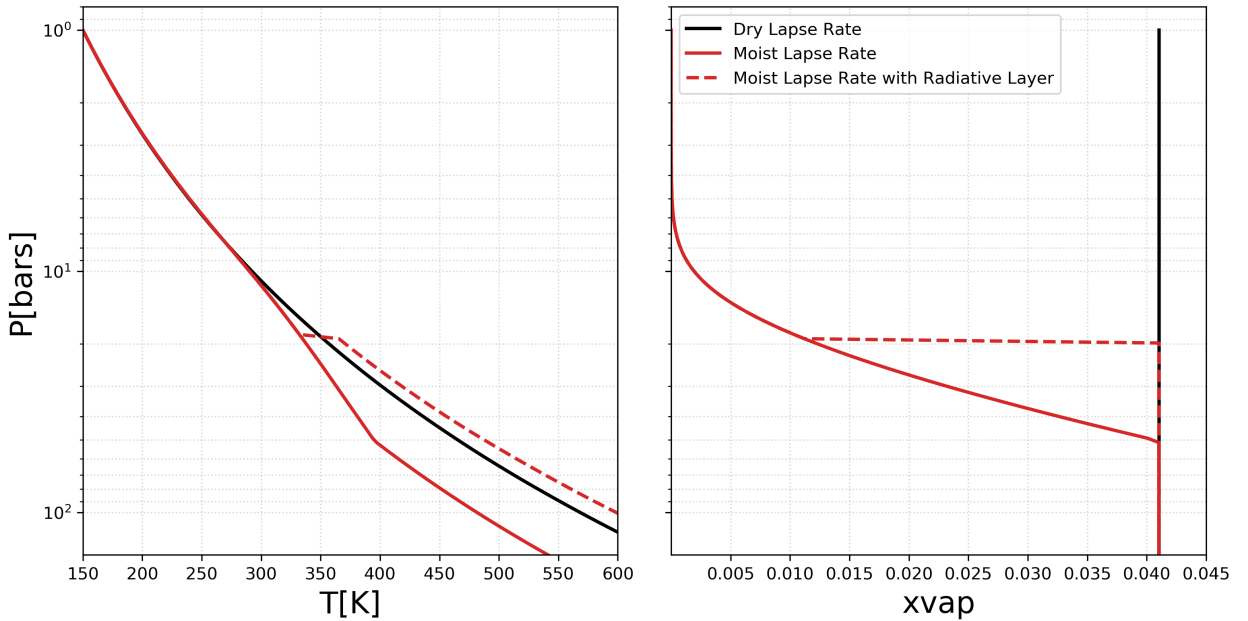


**Figure 2.3:** The solid red line is the profile following moist adiabatic lapse rate. The solid black line is following the the dry adiabatic lapse rate. The dashed red line is following a moist adiabatic lapse rate with the addition of a stable radiative layer (water condensation zone).

$$\alpha = 1 + \xi(q_s L / R_{\text{vap}} T_0) \quad (2.14)$$

where  $R_{\text{vap}}$  is the gas constant for the vapor (water),  $T_0$  is the local temperature,  $L$  is the latent heat of vaporization for water,  $q_s$  is the saturation specific humidity, and  $\xi$  is given by  $\xi = \frac{1}{\epsilon} - 1$ , where  $\epsilon$  is the ratio of the molecular weight of vapor to the mean molecular weight of dry atmosphere. In our case,  $\xi \approx -0.872$ . When  $\alpha$  is negative, the vertical gradient in molecular weight results in a stabilizing effect, overwhelming the effects due to latent heat release.

## 2.3 Temperature Jump Across the Water Condensation Zone

In a layer in which alpha, Eqn. 2.14, becomes negative, convection is interrupted. In the limit that H<sub>2</sub>O rains out quickly, (Friedson & Gonzales, 2017; Leconte et al., 2017) it has been shown that radiative diffusion is responsible for heat transport, with the temperature gradient across the zone following a radiative temperature gradient (R. Kippenhahn, 2012)

$$\left(\frac{dT}{dP}\right)_{\text{rad}} = \frac{T}{P} \nabla_{\text{rad}} = \frac{T}{P} \times \frac{3}{16} \frac{\kappa_R P}{g} \frac{T_{\text{int}}^4}{T^4} \quad (2.15)$$

Due to the large opacities,  $\kappa_R$ , that are typical of giant planet interiors, the radiative gradient is significantly larger than the either the dry adiabatic gradient or moist adiabatic gradient. This radiative gradient results in a sharp temperature increase as seen with the dashed-red curve in Figure 2.3. Since our model has a finite radial resolution, it is unable to spatially resolve the temperature change. Instead, the model treats the water condensation zone (a thin, stable, radiative layer) as a discontinuous increase in temperature. Nevertheless, this radiative zone corresponds to a continuum of temperatures that is governed by

$$T(P) = T_{\text{top}} + \int_{P_{\text{top}}}^{P_{\text{base}}} \left(\frac{dT}{dP}\right)_{\text{rad}} dP \quad (2.16)$$

with  $P_{\text{top}}$  and  $T_{\text{top}}$  denote the pressure and temperature at the top of the stable water condensation zone, and  $P_{\text{base}}$  represents the bottom of the zone. The radiative temperature gradient across the water condensation zone is nearly constant, so that Eqn. 2.16 simplifies to

$$T_{\text{base}} \equiv T(P + \Delta P) = T_{\text{top}} + \left(\frac{dT}{dP}\right)_{\text{rad}} \Delta P \quad (2.17)$$

where  $\Delta P$  is the extent of the pressure-space of the water condensation zone (radiative layer), given by

$$\Delta P \equiv P_{\text{base}} - P_{\text{top}} = \frac{P_{\text{sat}}(T_{\text{base}})}{x_{\text{vap}}^{\text{deep}}} - P_{\text{top}}. \quad (2.18)$$

Within the condensation zone, the vapor mole fraction,  $x_{\text{vap}}$  is equal to the saturated vapor mole fraction:

$$x_{\text{vap}}(P, T) = x_{\text{vap}}^{\text{sat}}(P, T) = \frac{P_{\text{sat}}(T)}{P}, \quad P < P_{\text{base}}. \quad (2.19)$$

The base of the condensation zone is set by the condition that  $x_{\text{vap}}$  has reached the deep value  $x_{\text{vap}}^{\text{deep}}$ :

$$x_{\text{vap}}^{\text{sat}}(P_{\text{base}}, T_{\text{base}}) = \frac{P_{\text{sat}}(T_{\text{base}})}{P_{\text{base}}} = x_{\text{vap}}^{\text{deep}}. \quad (2.20)$$

Below the water condensation zone, the region is subsaturated and hence no condensation occurs. Temperatures below the water condensation zone are obtained by integrating the dry adiabat  $\nabla_{\text{ad}}$

$$T(P > P_{\text{base}}) = T_{\text{base}} + \int_{P_{\text{base}}}^P \left( \frac{dT}{dP} \right)_{\text{ad}} dP. \quad (2.21)$$

## 2.4 Energy Conservation and Thermal Evolution of Model

Conservation of energy implies that the planet's luminosity, given by

$$L_{\text{int}} = 4\pi R^2 \sigma_{\text{SB}} T_{\text{int}}^4 \quad (2.22)$$

must be balanced by the rate of change of its total internal energy. When we have a sequence of progressively cooler models, we calculate the timestep between any two models using the

energy conservation equation as in (Fortney et al., 2011)

$$\frac{dL}{dm} = -T \frac{\partial S}{\partial t} \quad (2.23)$$

where  $dm$  is the mass of the shell,  $\partial S$  is the entropy of the shell, and  $T$  is the temperature of the shell. Solving for  $\partial t$ , we get the timestep

$$\partial t = -\frac{1}{L} \int_0^M \partial S dm \quad (2.24)$$

# 3

# Results

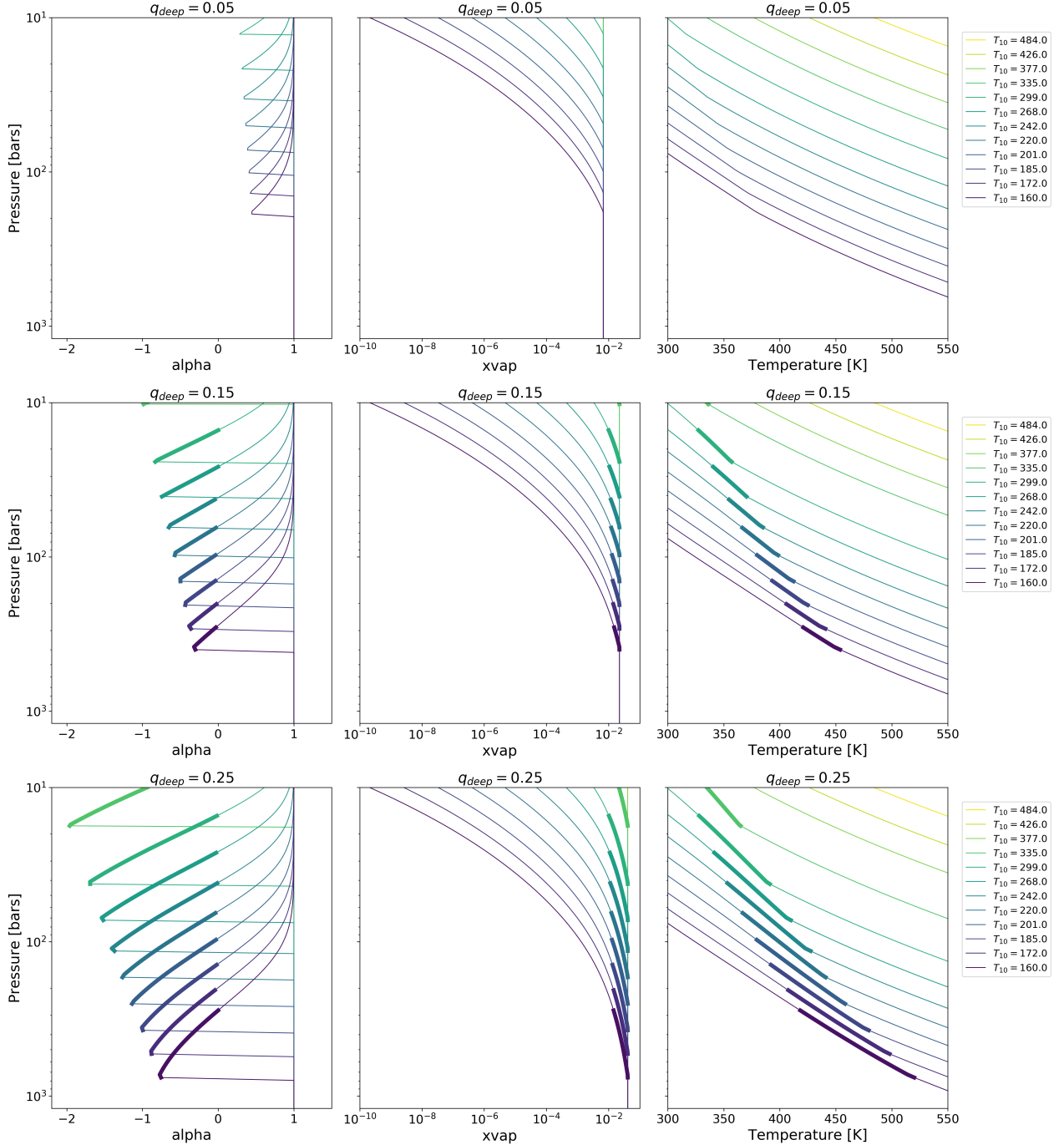
## 3.1 Condensation-inhibited Convection

Figure 3.1 shows the results of our initial, exploratory models. We show  $\alpha$  with respect to pressure, vapor mole fraction, and temperature. These static models are run for a variety of  $T_{10}$ 's, the planet's temperature at  $P = 10$  bars. As the bulk water abundance for Uranus and Neptune is unconstrained (Guillot, 1995), the model runs use three different values of  $q_{\text{deep}}$ , searching for deep water abundances and evolutionary phases for which convection is inhibited by water condensation. In these exploratory models, we only consider the model Uranus. We find that for  $q_{\text{deep}} = 0.05$ , no condensation-inhibited convection occurs. In other words,  $\alpha$  (Eqn. 2.14) never takes on negative values with this concentration of water vapor, hence the condition for stability is never met. However, for larger values of  $q_{\text{deep}}$ , we find that  $\alpha$  does take on negative values (see rows 2 and 3 in Figure 3.1). These finding are in agreement with (Friedson & Gonzales, 2017; Leconte et al., 2017). The shaded regions of the plots indicate the pressure-space over which  $\alpha$  is negative. For

these exploratory models, we neglected the stable water condensation zone's impact on the interior's thermal structure. More specifically, these profiles describe a scenario in which moist convection occurs throughout. As such, the shaded regions appear extended, when in reality the top of the shaded region indicates where the top of where the stable water condensation zone would form. As we will see in Section 2.3, self-consistent models that account for the formation of a stable zone, with a critical  $q_{\text{deep}}$ , will show pressure-temperature profiles with an abrupt temperature increase at the location of the radiative layer. Looking at the plots for  $q_{\text{deep}} = 0.15$  and  $q_{\text{deep}} = 0.25$ , we can see that condensation-inhibited convection sets in at approximately  $T_{10} = 335\text{K}$ . With regard to the xvap panels on the right of Figure 3.1, we can see that for a hot model Uranus, xvap profiles are vertical, taking on a constant value. For cooler Uranus models, we see that as water condenses out, xvap decreases. In the temperature-pressure profiles, we can see a kink in the graphs, corresponding to xvap taking on a constant value. In other words, the region has become sub-saturated and from that point, the profile follows a dry adiabat. Finally, we can see that as the planet cools, the condensation zones descend deeper into the interior.

### 3.2 Formation of Radiative Zone

Now we turn our focus to static models that explicitly allow for the formation of stable water condensation zones when conditions are suitable, as determined by the stability criterion, described by Eqn. 2.14. The plots in Figure 3.3 show the temperature profile and vapor mole fraction for H<sub>2</sub>O for three different values of  $q_{\text{deep}}$ : 0.05, 0.15, and 0.25. In the first row, we can see that for early  $T_{10}$ 's, there is no onset of condensation, and the profile follows a dry adiabat. For later  $T_{10}$ 's, there is a visible kink in the lapse rate



**Figure 3.1:** Each row represents a different value for  $q_{deep}$ . For  $q_{deep} = 0.05$ , no stable condensation zone forms. For  $q_{deep} = 0.15$  and  $q_{deep} = 0.25$ , convection is inhibited by condensation. The shaded regions show the extent of when  $\alpha$  is negative.

which indicates the onset of condensation, at which point the lapse rate has a shallower slope. For the larger values of  $q_{\text{deep}}$ , where  $\alpha$  takes on negative values, we see the onset of condensation-inhibited convection and the establishment of a radiative zone. In the plots, the water condensation zones are represented by the horizontal discontinuities moving from left to right. As the planet cools, these radiative zones descend deeper into the planet's interior. When the radiative zones are established, the interior below the zone becomes much warmer. In Figure 3.2, we highlight the effect of a warming interior. In this figure, we have overlaid the profiles for  $q_{\text{deep}} = 0.25$  (exhibiting stable water condensation zones) over the profile for  $q_{\text{deep}} = 0.05$  (no stable zones). From this plot, one can see that the presence of a radiative zone creates a temperature jump such that a given  $T_{10}$  appears to look like an earlier  $T_{10}$ . In other words, we find that the steep temperature increase caused by the presence of a radiative zone causes the interior to be much hotter than one would find using a simple moist adiabatic model with no stable layers. So, for a fixed  $T_{10}$ , while sub-critical( $q_{\text{deep}}=0.05$ ) and super-critical ( $q_{\text{deep}}=0.25$ ) models may appear identical near the surface, the super-critical model has a much warmer interior, one that resembles an earlier evolutionary track at a higher  $T_{10}$ .

Looking at the adjacent  $x_{\text{vap}}$  plots, we can see that  $x_{\text{vap}}$  follows its saturated value. At the bottom of the radiative zone, the vapor mole fraction equals its deep water value, which is the condition that sets the base of the condensation zone.

### 3.3 Thermal Evolution of Uranus and Neptune

In Figure 3.4, we display the results of evolutionary tracks that consider separately the evolution of a dry adiabat, a moist adiabat with condensation but no stable radiative

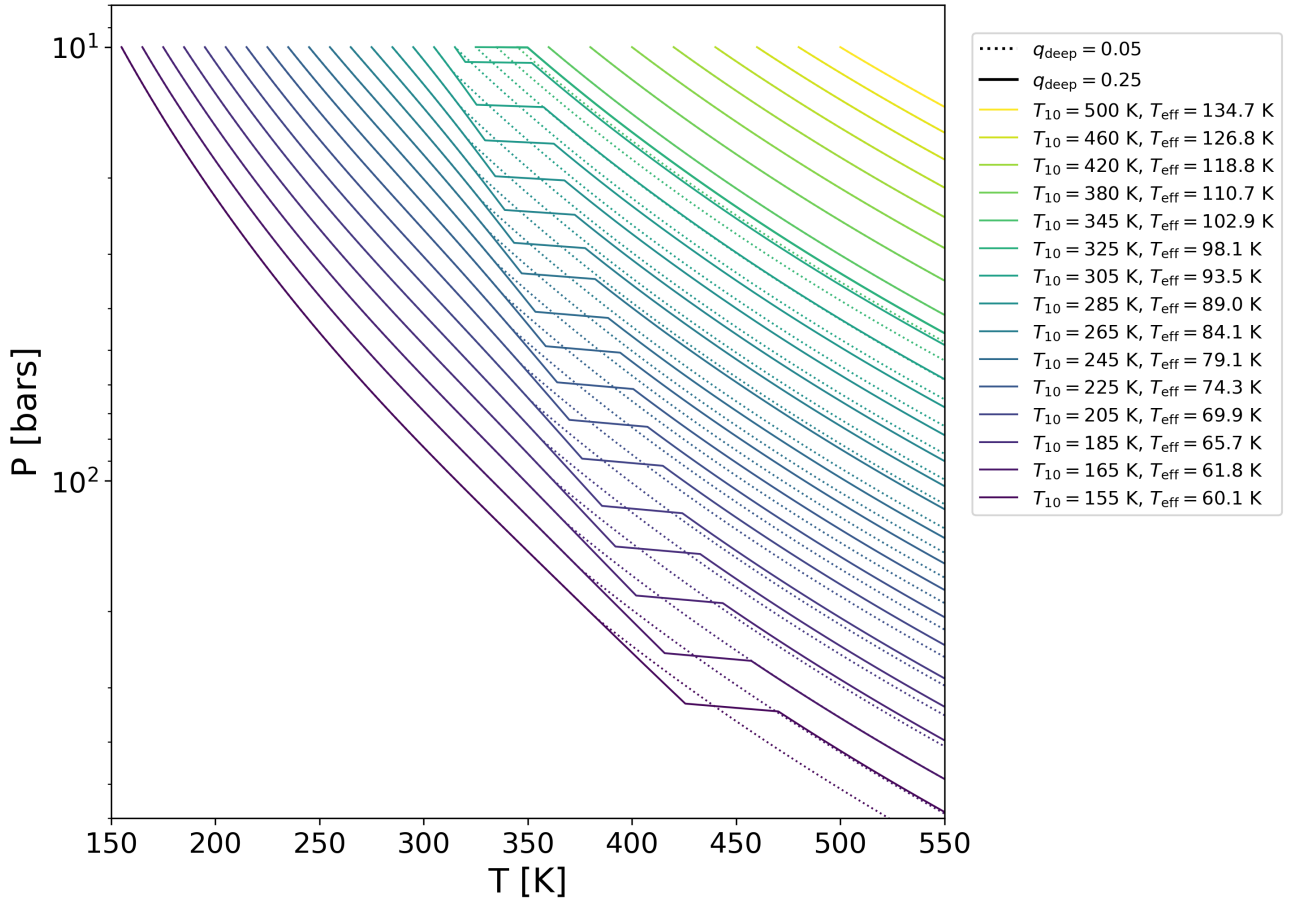


**Figure 3.2:** The solid lines represent the pressure-temperature profile for  $q_{\text{deep}} = 0.25$ , and the dashed lines for  $q_{\text{deep}} = 0.05$ . Looking at recent  $T_{10}$ 's, interior temperatures for  $q_{\text{deep}} = 0.25$  jump to an earlier  $T_{10}$ .

zone, and a moist adiabat with condensation containing stable radiative zones. For all of these evolutionary tracks, we assume  $q_{\text{deep}} = 0.25$ . Looking at these evolutionary tracks, the coolest scenario at present time, is a moist adiabat that is never stable against convection. The moist adiabat that is stable against convection has the warmest outcome at present time. In Figure 3.5 (Uranus) and Figure 3.6 (Neptune), we consider the impact of different deep water concentrations on the thermal evolution of Uranus and Neptune. As the planets cool, their radiative zones descend deeper into the interior, as we saw in Figure 3.3. This

behavior is also noticeable in the thermal evolution plots. Looking at  $T_{\text{eff}}$  at  $7 \times 10^7$  Gyr, the onset of condensation-inhibited convection occurs, resulting in a discontinuous temperature drop. The same behavior is seen in the  $T_{10}$  plots for both planets, however, by this time the radiative zone has descended deeper, later in time at around  $7 \times 10^8$  Gyr. Larger  $q_{\text{deep}}$ 's result in warmer Uranus and Neptune at present time. We also look at the impact of  $q_{\text{deep}}$  on the evolution of planetary radius and find that larger values of  $q_{\text{deep}}$  tend to converge more closely toward the presently observed radius for both Uranus and Neptune in these simulations.

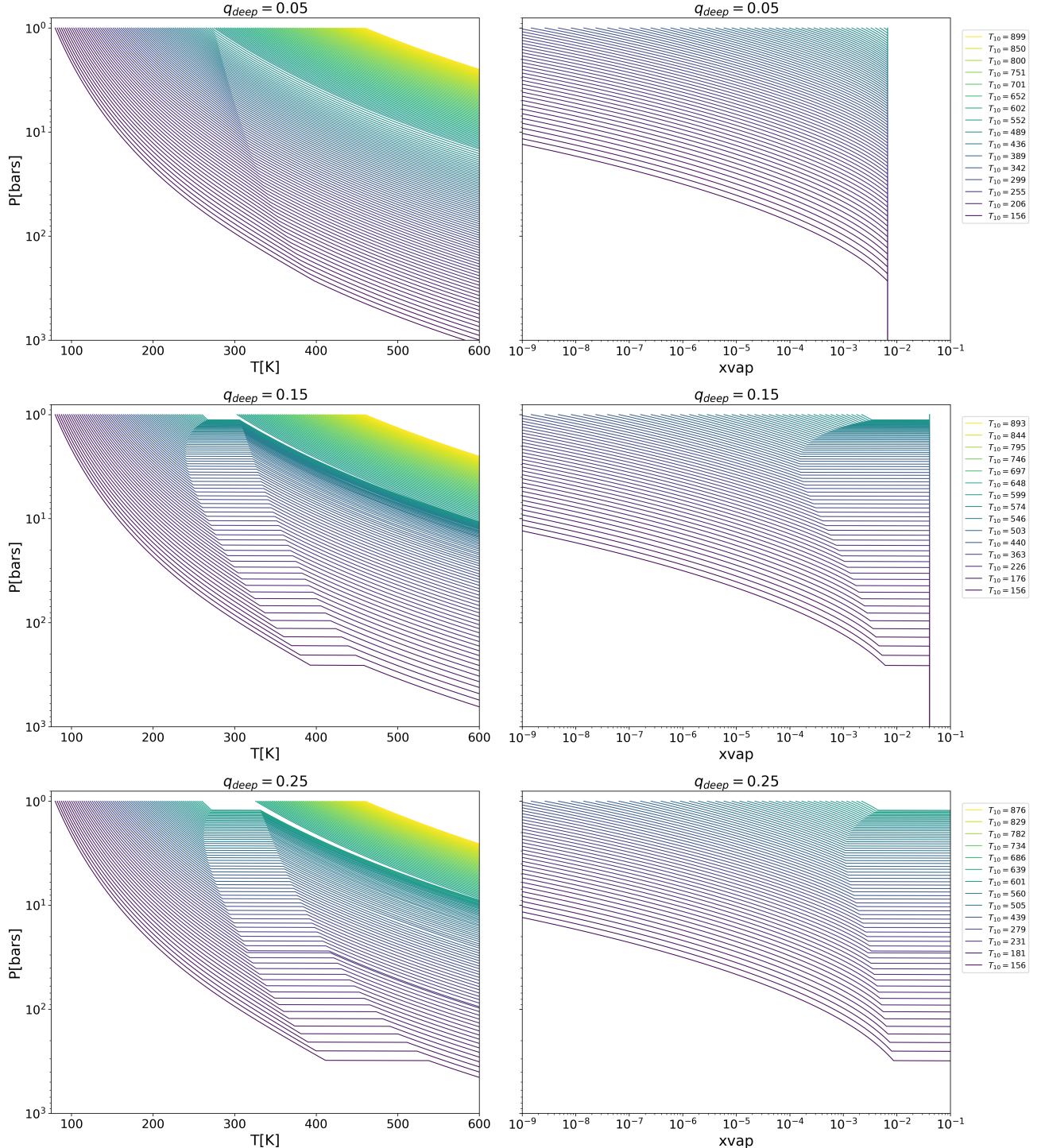


**Figure 3.3:** These plots were generated using our model Uranus. Again, from top to bottom, we move from  $q_{\text{deep}} = 0.05$ , 0.15, and 0.25, respectively.  $T_{10}$ 's range from hotter (yellow) to cooler (purple), more recent temperatures. For  $q_{\text{deep}} = 0.05$ , no stable radiative zones are formed. The kink visible in the middle of the top left plot represents the transition from a moist to dry adiabat. Condensation occurs, but no stability is achieved. For  $q_{\text{deep}} = 0.15$  and  $q_{\text{deep}} = 0.25$ , stable radiative zones are formed, as indicated by the discontinuous temperature jumps moving left to right.

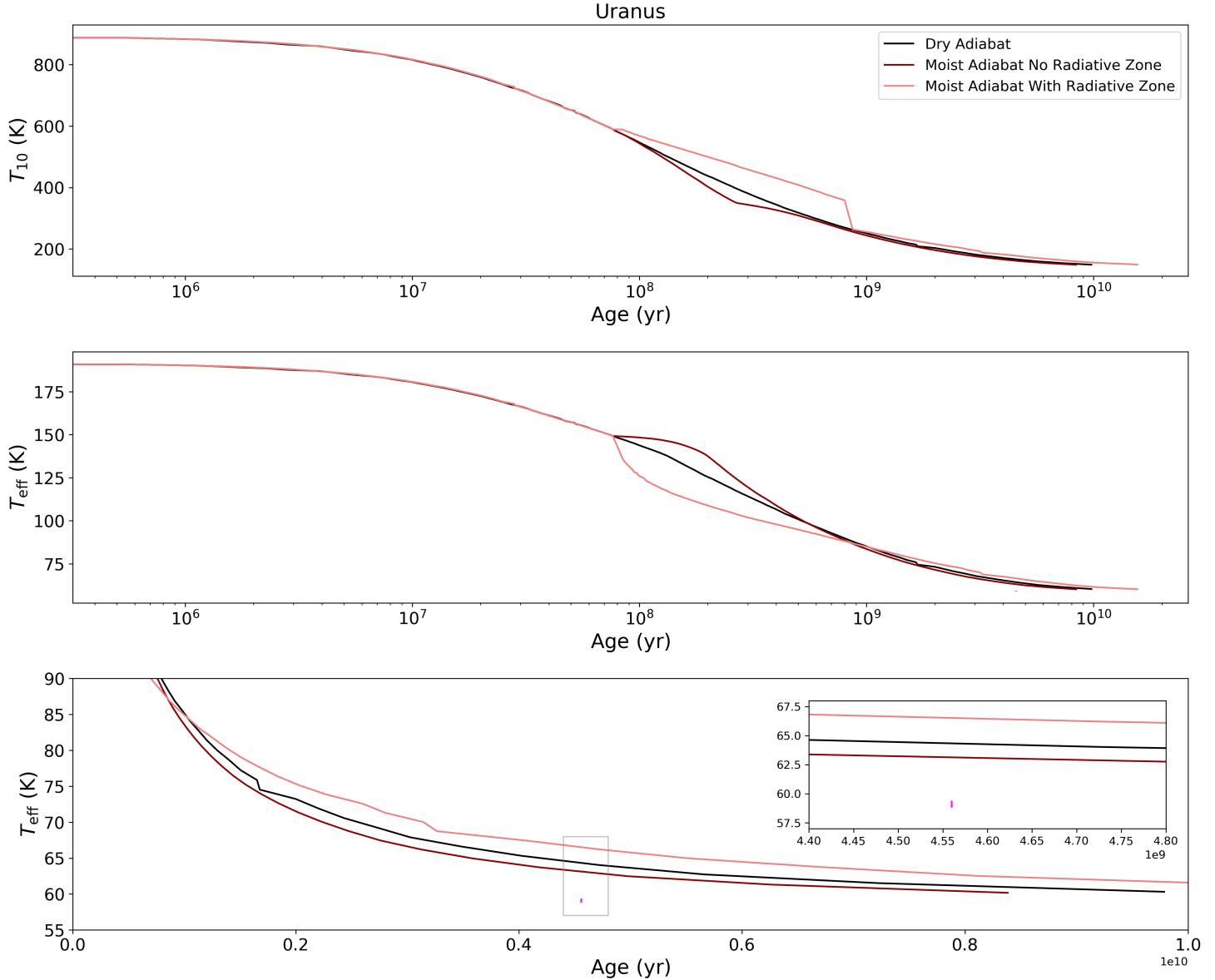


**Figure 3.4:** The black line represents the thermal evolution for a dry adiabat. The dark red line represents the thermal evolution for a moist adiabat that does not allow for the formation of a stable radiative layer. The light red line represents the thermal evolution of a moist adiabat that does allow for the formation of a stable radiative zone. The fuchsia dot on the lower plot represent the currently observed effective temperature of Uranus with error range.

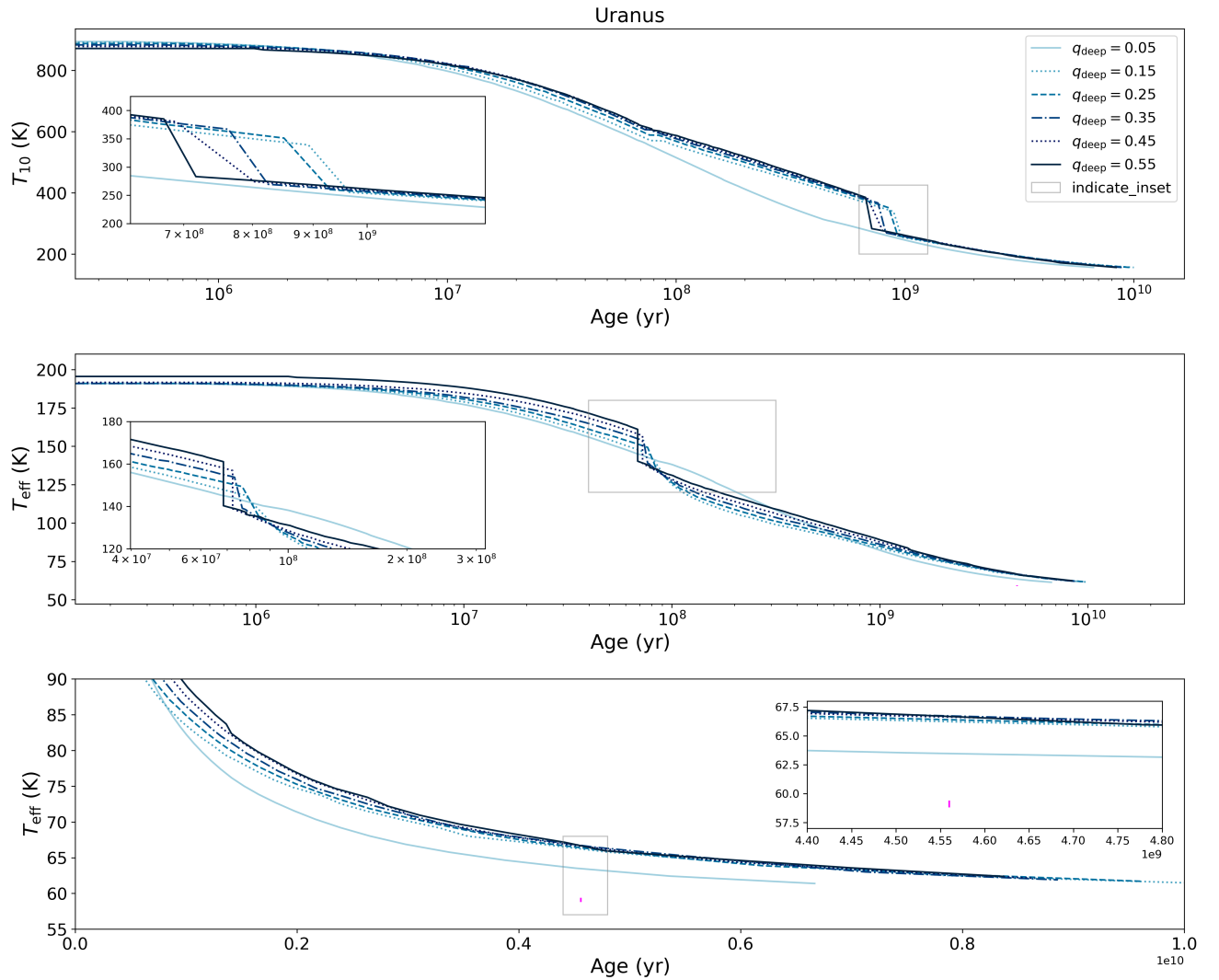


**Figure 3.5:** The curves in these plots represent thermal evolution tracks for different values of  $q_{\text{deep}}$ . Dark blue is the largest concentration of water vapor, at  $q_{\text{deep}} = 0.55$  and the light blue line is the least concentration of water vapor at  $q_{\text{deep}} = 0.05$ . For  $q_{\text{deep}} = 0.05$ , there is no onset of condensation-inhibited convection and no rapid cooling episode. For larger values of  $q_{\text{deep}}$  there is a rapid cooling episode for  $T_{\text{eff}}$  at around  $7 \times 10^7$  Gyr. Similarly, a rapid cooling episode is visible deeper down in the interior as seen in the  $T_{10}$  curves at around  $8 \times 10^8$  Gyr. The insets zoom in on periods of rapid cooling. The vertical fuchsia line represents the current  $T_{\text{eff}}$  with error range.

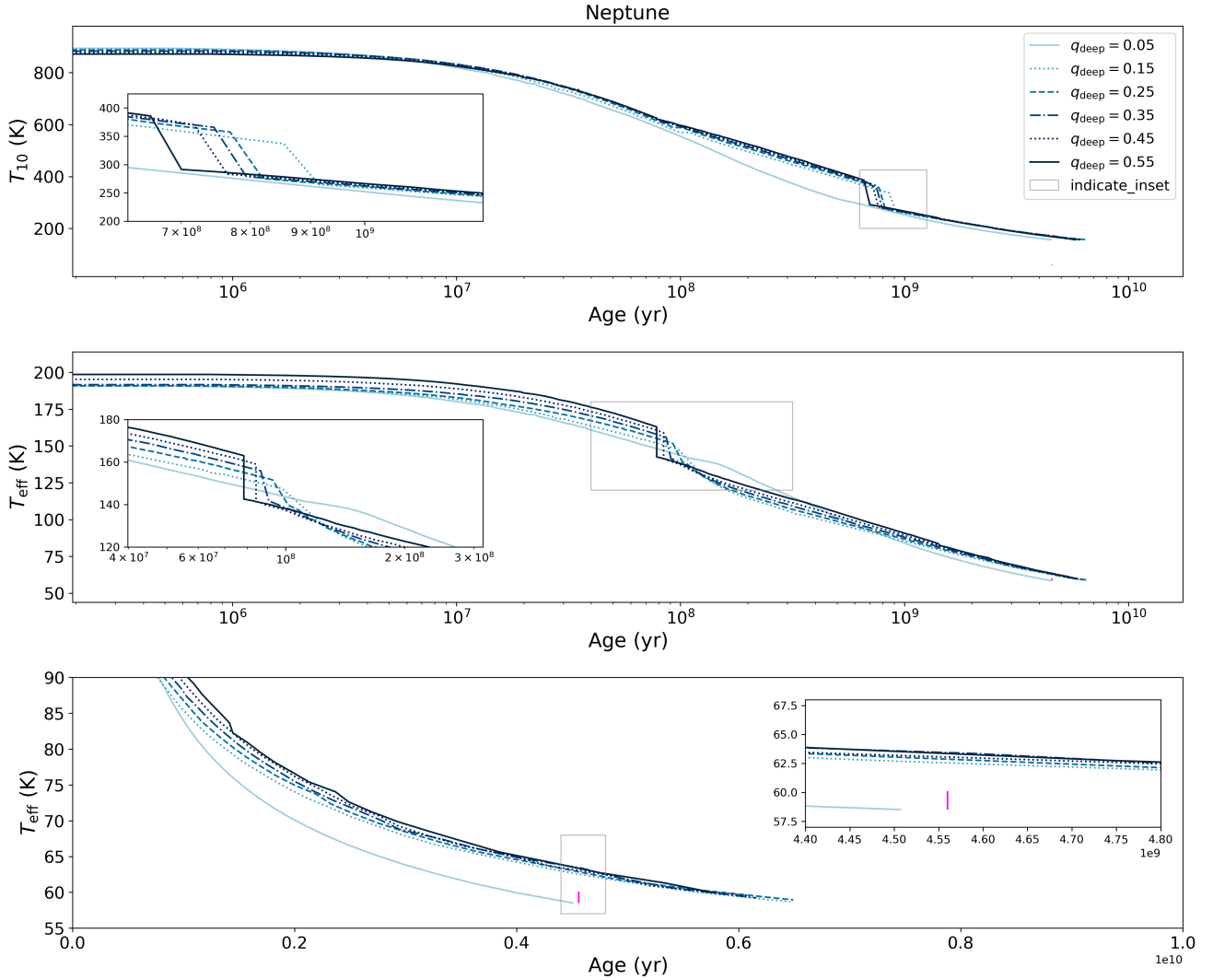


**Figure 3.6:** Similar to the Uranus plots, The curves in these plots represent thermal evolution tracks for different values of  $q_{\text{deep}}$ . Dark blue is the largest concentration of water vapor, at  $q_{\text{deep}} = 0.55$  and the light blue line is the least concentration of water vapor at  $q_{\text{deep}} = 0.05$ . For  $q_{\text{deep}} = 0.05$ , there is no onset of condensation-inhibited convection and no rapid cooling episode. For larger values of  $q_{\text{deep}}$  there is a rapid cooling episode for  $T_{\text{eff}}$  at around  $7 \times 10^7$  Gyr. Similarly, a rapid cooling episode is visible deeper down in the interior as seen in the  $T_{10}$  curves at around  $8 \times 10^8$  Gyr. The insets zoom in on periods of rapid cooling. The vertical fucshia line represents the current  $T_{\text{eff}}$  with error range.

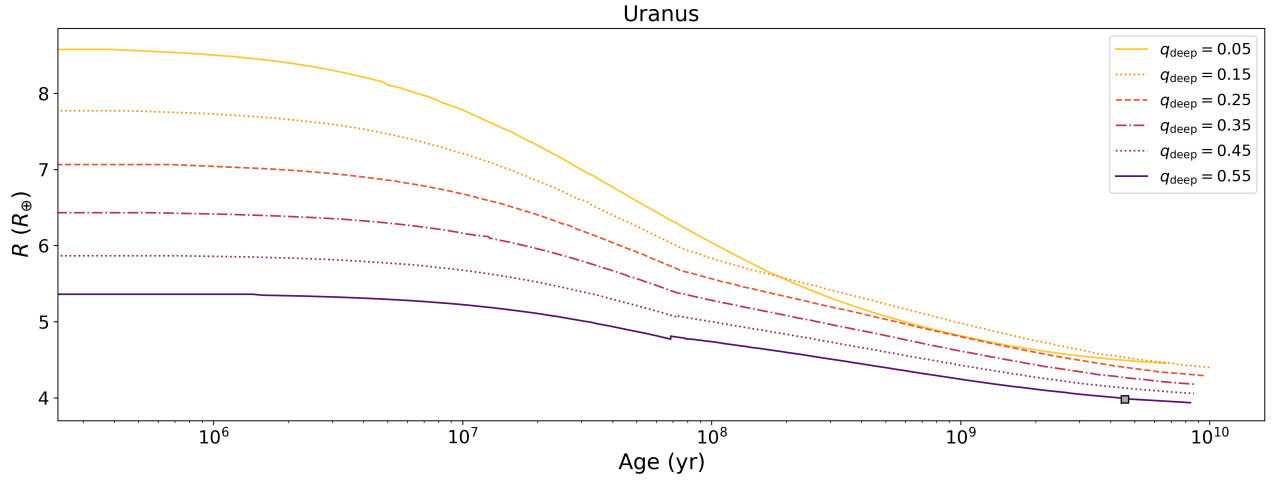


**Figure 3.7:** This thermal evolution plot shows the impact of different deep water concentration on the radius on model Uranus as it cools. The gray square represents the current observed radius.

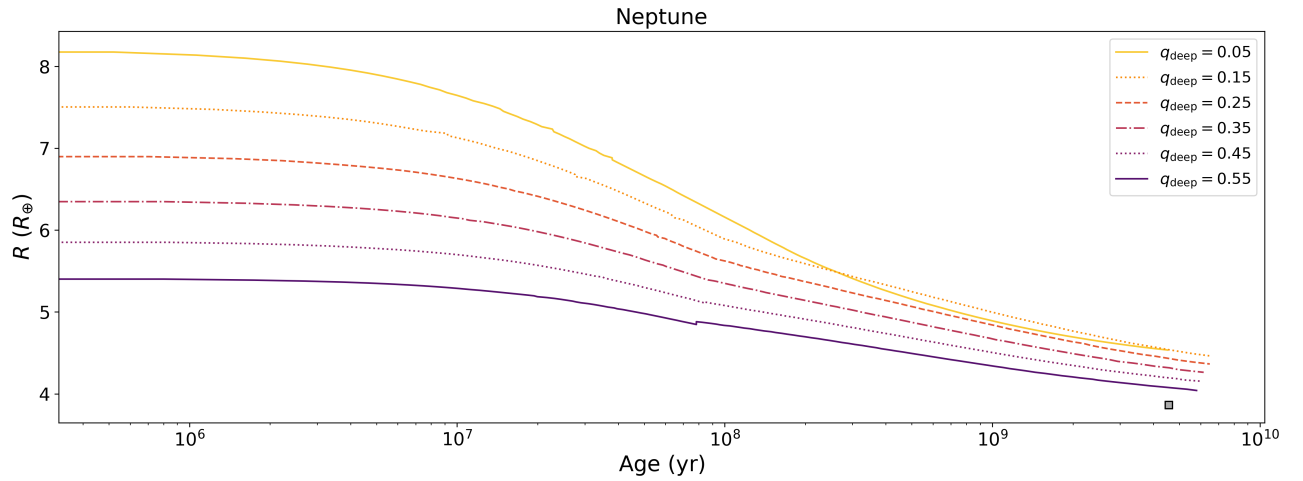


**Figure 3.8:** This thermal evolution plot shows the impact of different deep water concentration on the radius on model Neptune as it cools. The gray square represents the current observed radius.

**4**

## Discussion and Conclusions

We set out to investigate the impact of water condensation zones on the thermal evolution of our solar system ice giants. It has been speculated that such thermal boundary layers could act as an imperfect insulator, trapping heat below and allowing the envelope above the boundary layer to cool more rapidly (Nettelmann et al., 2016)(Friedson & Gonzales, 2017)(Leconte et al., 2017)(M. Podolak, 1991)(L. Scheibe, 2019). It seems plausible that such interiors could explain the problem with Uranus appearing to have no intrinsic temperature. And, while our analysis suggests that moist-adiabatic interiors have a significant impact on the heat flow and thermal evolution of ice giants, making a case for the inclusion of moist adiabats in contemporary interior structure models, our findings are nonetheless inconclusive on the problem of Uranus. We do find that incorporating a moist adiabat into our interior structure model does result in a cooler model Uranus and Neptune than would otherwise be seen with a purely dry model. However, when we add stable radiative zones to the interior, we find in the planet's past a period of rapid cooling that results in a cooler effective temperature at around  $7 \times 10^7$  Gyr. However, both model

Uranus and model Neptune eventually become warmer at present time than predicted by either dry or simple moist adiabatic models. It is possible that reality resembles something in between the binary choice of an atmosphere with a moist adiabat containing a thermal boundary layer or an atmosphere with a moist adiabat containing no thermal boundary layer (Guillot, 2020). Our assumption of a stable shell of water condensation assumes that there are no other dynamics at play, such as upwelling or entrainment pressure (Friedson & Gonzales, 2017) eroding and punching holes in the stable radiative zone. Such a scenario could plausibly allow for more mixing of the warm gases below and above the condensation zone. Additionally, we considered only one condensate, H<sub>2</sub>O. It would be worth considering NH<sub>3</sub> and CH<sub>4</sub>, and analyzing the impact of multiple stratified layers on the cooling of the planet over time. To summarize, future work should consider: 1.) Impact of entrainment pressure on stable water condensation zones. 2.) The possibility of porous condensation zones. 3.) The formation of multiple concurrent thermal boundary layers formed from different condensates.

# Bibliography

- Chabrier, G., Mazevet, S., & Soubiran, F. (2019). A New Equation of State for Dense Hydrogen-Helium Mixtures. *Astrophysical Journal*, 872(1), 51.
- Demarcus, W. C. (1958). The constitution of Jupiter and Saturn. *Astronomical Journal*, 63, 2.
- Fortney, J. J. & Hubbard, W. B. (2003). Phase separation in giant planets: inhomogeneous evolution of Saturn. *Icarus*, 164(1), 228–243.
- Fortney, J. J., Ikoma, M., Nettelmann, N., Guillot, T., & Marley, M. S. (2011). Self-consistent Model Atmospheres and the Cooling of the Solar System’s Giant Planets. *Astrophysical Journal*, 729(1), 32.
- Friedson, A. J. & Gonzales, E. J. (2017). Inhibition of ordinary and diffusive convection in the water condensation zone of the ice giants and implications for their thermal evolution. *Icarus*, 297, 160–178.
- Graboske, H. C., J., Pollack, J. B., Grossman, A. S., & Olness, R. J. (1975). The structure and evolution of Jupiter: the fluid contraction stage. *Astrophysical Journal*, 199, 265–281.

- Guillot, T. (1995). Condensation of Methane, Ammonia, and Water and the Inhibition of Convection in Giant Planets. *Science*, 269(5231), 1697–1699.
- Guillot, T. (2020). Uranus and Neptune are key to understand planets with hydrogen atmospheres. In *European Planetary Science Congress* (pp. EPSC2020–514).
- Hubbard, W. B. (1968). Thermal structure of Jupiter. *Astrophysical Journal*, 152, 745–754.
- Hubbard, W. B. (1977). The Jovian Surface Condition and Cooling Rate. *Icarus*, 30(2), 305–310.
- Hubbard, W. B. (1978). Comparative thermal evolution of Uranus and Neptune. *Icarus*, 35(2), 177–181.
- L. Scheibe, N Nettelmann, R. R. (2019). Thermal evolution of uranus and neptune: Adiabatic models. *Astronomy and Astrophysics*, A70, 632.
- Lavega, A. S. (2011). Introduction to planetary atmospheres.
- Leconte, J. & Chabrier, G. (2013). Layered convection as the origin of Saturn’s luminosity anomaly. *Nature Geoscience*, 6(5), 347–350.
- Leconte, J., Selsis, F., Hersant, F., & Guillot, T. (2017). Condensation-inhibited convection in hydrogen-rich atmospheres . Stability against double-diffusive processes and thermal profiles for Jupiter, Saturn, Uranus, and Neptune. *Astronomy and Astrophysics*, 598, A98.
- Low, F. J. (1966). Observations of Venus, Jupiter, and Saturn at  $\lambda 20 \mu$ . *Astronomical Journal*, 71, 391.

- M. Podolak, W.B. Hubbard, D. S. (1991). Models of uranus' interior and magnetic field. *Uranus, Editors: J.T. Bergstrahl, E.D. Miner, M. Shapely Matthews*, (pp.29).
- Mankovich, C. & Fortney, J. J. (2019). Evidence for a Dichotomy in the Interior Structures of Jupiter and Saturn from Helium Phase Separation. In *AGU Fall Meeting Abstracts*, volume 2019 (pp. P24B–02).
- Nettelmann, N., Wang, K., Fortney, J. J., Hamel, S., Yellamilli, S., Bethkenhagen, M., & Redmer, R. (2016). Uranus evolution models with simple thermal boundary layers. *Icarus*, 275, 107–116.
- Pearl, J. C. & Conrath, B. J. (1991). The albedo, effective temperature, and energy balance of Neptune, as determined from Voyager data. *Journal of Geophysical Research*, 96, 18921–18930.
- R. Kippenhahn, A. Weigert, A. W. (2012). *Stellar Structure and Evolution*. Springer.
- S. Mazevet, A. Licari, G. C. & Potekhin, A. Y. (2019). Ab initio based equation of state of dense water for planetary and exoplanetary modeling. *Astronomy & Astrophysics*, A128, 621.
- Seager, S. (2010). Exoplanet atmospheres.
- Smoluchowski, R. (1967). Internal Structure and Energy Emission of Jupiter. *Nature*, 215(5102), 691–695.
- W.B. Hubbard, D. S. (1995). The interior of neptune. *Neptune and Triton, Editor: D.P. Kruikshank*, (pp. 109).